Drug Development and Industrial Pharmacy

ISSN: (Print) (Online) Journal homepage: https://www.tandfonline.com/loi/iddi20

Microneedles assisted controlled and improved transdermal delivery of high molecular drugs via *in situ* forming depot thermoresponsive poloxamers gels in skin microchannels

Samiullah Khan, Muhammad Usman Minhas, Raghu Raj Singh Thakur & Muhammad Tahir Aqeel

To cite this article: Samiullah Khan, Muhammad Usman Minhas, Raghu Raj Singh Thakur & Muhammad Tahir Aqeel (2022): Microneedles assisted controlled and improved transdermal delivery of high molecular drugs via *in situ* forming depot thermoresponsive poloxamers gels in skin microchannels, Drug Development and Industrial Pharmacy, DOI: 10.1080/03639045.2022.2107662

To link to this article: https://doi.org/10.1080/03639045.2022.2107662

DRUG DEVELOPMENT AND INDUSTRIAL PHARMACY
https://doi.org/10.1080/03639045.2022.2107662

Taylor & Francis
Taylor & Francis Group

RESEARCH ARTICLE

Microneedles assisted controlled and improved transdermal delivery of high molecular drugs via *in situ* forming depot thermoresponsive poloxamers gels in skin microchannels

Samiullah Khan[a], Muhammad Usman Minhas[b], Raghu Raj Singh Thakur[c] and Muhammad Tahir Aqeel[a]

[a]Margalla College of Pharmacy, Margalla Institute of Health Sciences, Rawalpindi, Pakistan; [b]School of Pharmacy, University of Sargodha, Sargodha, Pakistan; [c]School of Pharmacy, Queen's University Belfast, Belfast, UK

ABSTRACT

Skin is considered as an attractive route for variety of drug molecule administration. However, it is proved to be the main physical barrier for drug flux owing to their poor permeability and low bioavailability across *stratum corneum* layer. In the current study, novel approach has been used to enhance transdermal delivery via microporation through combination of poloxamers gels and microneedles (MNs) arrays. The phase transition of poloxamers at various concentrations from sol–gel was evaluated using AR2000 rheometer to confirm MNs-assisted *in situ* forming depots. Temperature test confirmed gelation between 32 and 37 °C. Curcumin was loaded in poloxamer formulations at variable concentrations and its effect showed reduction in critical gelation temperature (CGT) owing to its hydrophobic nature. Microneedle arrays (600 μm) prepared from Gantrez S-97, PEG10000 and gelatin B using (19 × 19) laser-engineered silicone micromoulds showed high mechanical stability investigated via Texture analyzer. From *in situ* dissolution profile, gelatin 15% w/w based MNs displayed quicker dissolution rate in comparison to PG10000. VivoSight® OCT scanner and dye tracking confirmed that PG10000 MNs arrays pierced SC layer, infiltrate the epidermis and goes to dermis layer. From *in vitro* permeation, it was concluded that 20% w/w PF127® gel formulations containing (0.1% and 0.3%) curcumin displayed high curcumin permeation for comparatively longer time through microporated skin samples in comparison to non-microporated skin. The curcumin distribution in skin tissues with higher florescence intensity was noted in MNs treated skin samples by confocal microscopy. FTIR confirmed the structure formation of fabricated MNs, while TGA showed dry, brittle and rigid nature of gelatin MNs.

ARTICLE HISTORY
Received 21 February 2022
Revised 23 July 2022
Accepted 25 July 2022

KEYWORDS
Poloxamers; Gantrez® S-97; curcumin; microneedles; PEG10000; *in situ* depots; confocal microscopy

Introduction

Microneedle (MN) arrays are minimally invasive micron scale biomedical devices which bypass the skin's outermost layer, the stratum corneum (SC), a major barrier to dermal agents without causing pain. These MNs form the interstitial fluid filled microchannels in the skin by passing through SC and grants the access to dermal microcirculation but less adequate not to effect the nerve endings of dermis layer and sensation of pain [1,2]. MNs are tiny needle like projections with length about 15–2000 μm in height and micron size in diameters positioned on baseplate in various geometries [3]. MN arrays have been used to make possible transdermal and intradermal delivery of variety of substances such as insulin, vaccines [4], cosmeceuticals [5], ovalbumin [6], low molecular weight heparin [7], sulforhodamine B [8], adenovirus vector [9], and monoclonal antibody [10]. Currently, researchers are paying great attention toward MNs technology owing to their possession of number of advantages over traditional drug delivery methods. Some benefits of MN arrays include painless administration of bioactive molecules, bypass first pass effect and delivery of range of pharmaceutical agents.

'Poke with patch' is considered to be the first technique utilized for transdermal MN-mediated delivery [11]. To date, different types of MN arrays have been reported in the literature. These MN arrays have been synthesized from materials such as stainless steel, glass, titanium, silicon, maltose, and polymers in different forms (coated, solid, hollow, and dissolvable), dimensions and densities [12,13]. Dissolvable MN arrays are promising alternative strategy for the rapid transdermal macromolecules and gene delivery. They should have significant sufficient robustness and mechanical strength for puncturing the skin to create the microchannels [14]. Dissolvable MNs are fabricated from a variety of biocompatible biopolymers such as sodium hyaluronate, chondroitin sulfate, poly(methyl vinyl ether-maleic anhydride, Gantrez® AN-139), sucrose, carboxymethylcellulose (CMC), polyglycolic acid (PGA), maltose, etc. [15,16]. Currently, MN arrays treated *in situ* forming depots are gaining significant interest and are considered novel alternate strategy for the delivery of different pharmaceutical agents with variable solubilities. These MN arrays fabricated from variety of polymers rupture the SC layer and form channels in the underlying layers for depots formation. To date, no significant work has been done and a very few studies have been reported on MN arrays treated *in situ* forming depots [17–19].

The thermoresponsive triblock copolymers, namely Pluronic® or Poloxamers representing a series of polyethyleneglycol-b-propyleneglycol-b-ethyleneglycol (PEO-PPO-PEO) units can exhibit reversible phase transition from sol–gel states as a result of water

CONTACT Samiullah Khan Sami_pharmacist99@hotmail.com Margalla College of Pharmacy, Margalla Institute of Health Sciences, Rawalpindi, Pakistan
Supplemental data for this article can be accessed online at https://doi.org/10.1080/03639045.2022.2107662.

uptake and release in aqueous solutions in response to temperature decrease and increase, respectively. The polymer solution exists as fluid below room temperature (<30 °C) and upon injection convert into semisolid hydrogel at physiological temperature and certain concentration [20,21]. Pluronics® are FDA approved biocompatible polymer that have been extensively investigated due to their unique thermogelation mechanism at skin (32 °C) and body temperature (37 °C) [22,23]. Recently, Khan et al. reported MNs assisted *in situ* forming poloxamers depots for sustained delivery of hydrophilic pharmaceuticals [17].

Gelatin is a biocompatible protein polymer made by partial hydrolysis of collagen sources from bones, cartilage, and ligaments [24]. Gelatin mainly contains the residues of three amino acids, glycine, proline, and 4-hydroxyproline in its structure [25]. Gelatin is FDA approved natural polymer preferred for its low toxicity and biocompatibility [26].

Curcumin, a natural low molecular weight yellow hydrophobic phytoconstituent is widely used as traditional medicine in China, India, and other Asian countries to treat various chronic diseases and inflammatory conditions [27,28]. Curcumin possesses antioxidant, anti-inflammatory, anti-tumorigenic, and hyperlipidemic activities. However, owing to its lowest water solubility (~11 ng/mL, pH), it exhibited poor oral availability and extensive first pass metabolism [29]. Another disadvantage associated with curcumin is its mode of applications, as administration of polyphenols in high concentrations may lead to severe toxic effects. So for the successful delivery and applications of curcumin, development of novel formulations with controlled release property is highly desired [30,31].

In this study, we report the formation of MNs assisted *in situ* forming hydrogel depots in the skin micro-channels using a range of poloxamers (poloxamer 407 or Pluronic® PF127 and poloxamer P87) and utilizing their temperature responsive sol–gel transition properties. Current study was based on the hypothesis that skin will be microporated by using optimized MN arrays followed by MNs assembly removal and application of drug loaded poloxamer solutions. The poloxamer drug containing solution will flow inside the pores and convert into depot at skin temperature (32 °C) gaining the MN shape and will provide controlled delivery of high molecular weight loaded molecules. In the current study, first different poloxamer grade solutions at variable concentrations were prepared and subjected to rheological analysis for the confirmation of sol–gel transition temperatures (32–37 °C). Then, 19 × 19 MN arrays (600 μm, height) were fabricated from aqueous solution of 15% w/w Gantrez S97/7.5% w/w, poly(ethyleneglycol) (PEG) 10,000 Da and 15% gelatin B. The MNs were screened for mechanical strength, *in situ* dissolution profile and moisture contents determination. The histology of piglet skin for pores creation by MN arrays application was investigated by dye tracking study and optical coherence tomography (OCT). The MNs insertion depth in hairless skin was also observed by OCT. The porcine skin barrier integrity was observed with trans-epidermal water loss (TEWL) before and after MNs treatment. Curcumin as a model pharmaceutical was loaded in optimized poloxamer solutions. To the best of our knowledge and as per literature review, to date, no study has been conducted for curcumin delivery through transdermal route using MNs assisted *in situ* forming hydrogel depots. The *in vitro* permeation of curcumin across skin samples was observed using vertical Franz's cell diffusion. Furthermore, confocal microscopy was used to track the biodistribution of curcumin in the skin layers. The MNs structural assessment was studied by Fourier transform infrared spectroscopy (FT-IR), while morphology of the MNs was assessed by scanning electron microscopy (SEM). Figure 1 refers to schematic diagram of *in situ* gel design and drug delivery from MNs assisted *in situ* forming gel depot.

Materials and methods

Materials

Gelatin type B (Ge) (Mw~403.47 g/mol) (Merck, Darmstadt, Germany), Pluronic® F-127 (MW 12,500 Da), Pluronic® F-87 (MW 7700 Da), and curcumin (Cur, purity = 99.97%) were purchased from BASF Chemical Company (Ludwigshafen, Germany). Gantrez®S-97 (Mw = 1500.000 Da), PEG (Mw = 10,000 Da).

Preparation of poloxamer solutions

Cold method was used for the preparation of poloxamer solutions. Different types of poloxamers (P127 and P87) at variable concentrations were slowly dispersed in cold distilled water (4 °C) at constant stirring to prepare poloxamer solutions. The solutions were placed for 24 h in the refrigerator to obtain clear solutions [17].

Preparation of curcumin loaded poloxamer solutions

For curcumin loaded poloxamer solutions, curcumin (0.1% and 0.3%) was first dissolved in small amount of methanol. The final volume of already prepared optimized poloxamer solutions was then made up with addition of curcumin solution at 20 °C under constant stirring. The final curcumin loaded poloxamer samples were then placed in the refrigerator till further use [17].

Rheological characterization

The thixotropic behavior of poloxamer solutions was observed with AR-2000 rheometer attached with circulating water bath for temperature control. The rheological characteristics of samples were studied by applying different tests in flow and oscillatory modes. In flow mode, viscosity change was analyzed under 0.1–10 1/s shear rate via continuous ramp test at 25 °C for 10 minutes. Temperature range test was used to evaluate viscosity behavior with temperature change (20–40 °C) at 1 rad/s frequency and 0.1 Pa shear rate. In oscillatory mode, elastic and viscous moduli (G' and G'') were observed in range of 20–40 °C temperature [32–34].

Fabrication of MN arrays

For MN arrays preparation, laser-engineered silicone micromould was used. The MNs mold contained 361 (19 × 19) needles of 600 μm average height. The arrays were fabricated from aqueous solutions of 15% w/w Gantrez S97, 7.5% w/w PEG and gelatin B (15% w/w). Briefly, 400 mg of polymer solutions were poured onto micromoulds and kept in centrifuge for 15 m. MN arrays were then kept for drying at room temperature for 48 h. After complete drying, the MN arrays were taken out of molds, placed in sealed container till further use [17,35].

Mechanical strength determination

The mechanical stability of fabricated MNs for compression and skin insertion was evaluated using TA-XT2 Texture analyzer under various compression forces. Before applying forces, MNs were scanned using Leica EZ4D digital microscope (Wetzlar, Germany). MNs were then fixed to the moveable probe with needles in

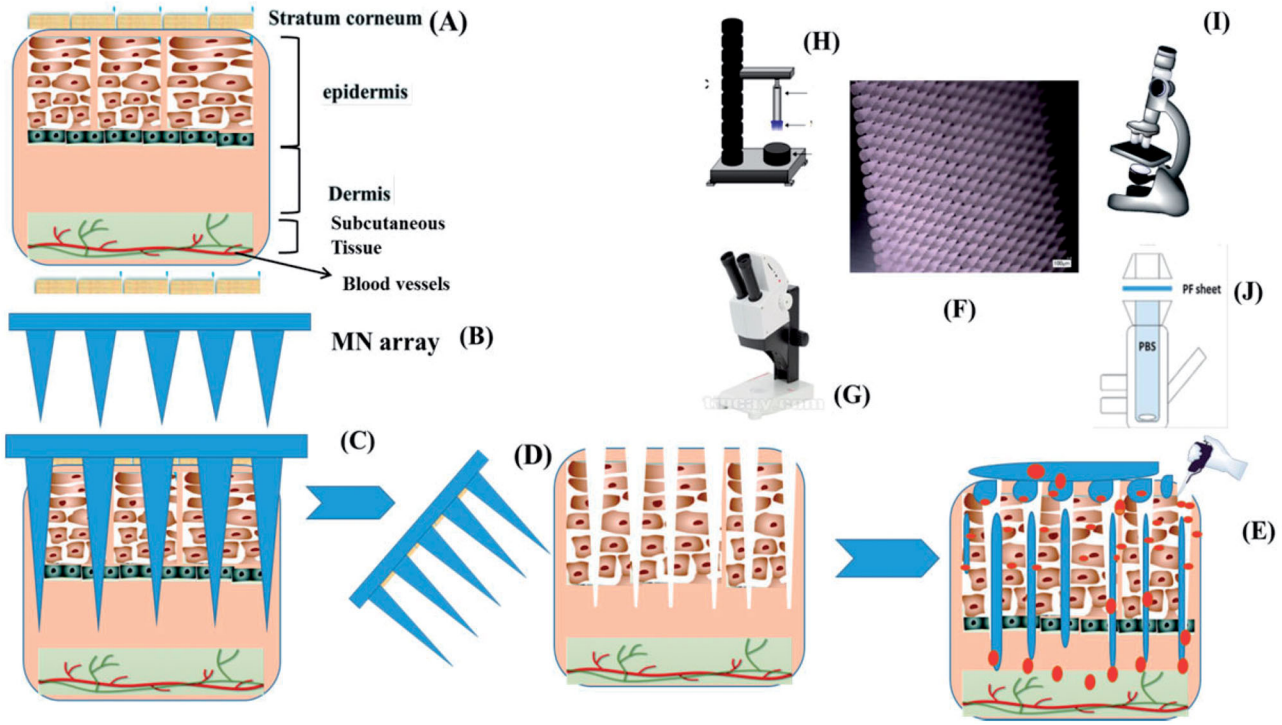

Figure 1. Schematic diagram of *in situ* gel design and drug release from MNs assisted *in situ* forming gel depot. Non-porated neonatal porcine skin (A), designing of MN arrays from various polymer blends (B), application of optimized MN arrays for pores creation in skin (C), pores formation in skin followed by MN arrays removal after predetermined time (D), application of drug-poloxamer solution on porated skin site, flow of drug-poloxamer solution, conversion into gel form at 32 °C and formation of *in situ* forming gel depot (E), digital image of optimized MN arrays prepared for pores creation in skin (F), Leica EZ4 D digital microscope (G), TA Texture analyzer setup for MNs mechanical strength determinations (H), confocal microscope for tracking drug distribution in skin tissues (I), and the Franz cell setup for *in vitro* permeation study (J).

downward directions. Texture analyzer probe was moved down at 0.1 mm/s speed till MNs touched the steel block and then started applying the pre-set forces. After reaching the target force for predetermined time, the probe is lifted up at same speed. MNs were viewed again after pre-set forces applications using the Leica EZ4 D digital microscope (Wetzlar, Germany) and the needle heights were calculated [13,17].

Skin insertion study

TA-XT2 Texture analyzer was utilized to observe the force required for MN arrays insertion in skin sample. The hairs on skin were carefully removed with disposable blade and sample was incubated in PBS (7.4) for 1 h at 37 °C. The sample was then fixed on dental wax sheet with its dermis side down. MN arrays were fixed to the probe of Texture analyzer. The probe of TA analyzer was lowered at 0.5 mm/s speed onto the skin for pre-set forces. As the probe reached the skin tissue, it pierced the SC barrier until the required force was reached [17,36].

Optical coherence tomography

OCT is a tool used to measure the depth of penetration and 2D visualization of MN insertion into skin. The hydrated skin samples previously incubated in PBS (pH 7.4) were placed on Styropor panel. An applicator device was used for MNs insertion in skin by applying 20 N force and visualized at once using VivoSight® high-resolution scanner. The skin layers were scanned up to 8B-scans per second [17,37].

In situ *MN arrays dissolution kinetics*

The *in situ* dissolution profile of fabricated MNs was investigated in skin samples. Briefly, previously prepared circular skin samples thawed in PBS (pH 7.4) for 30 min were attached to the donor compartment of the Franz diffusion cell at 37 ± 1 °C. Before *in situ* dissolution study, MN heights were measured. The MN arrays were inserted with applicator into the skin center section. At each interval, the MNs were detached and stored at −20 °C till viewing. MN arrays were viewed with Leica MZ6 microscope (Wetzlar, Germany) fixed with Nikon 950 digital camera (Minato City, Japan). During *in situ* dissolution, the change in MNs heights was calculated each time. All the measurements were made in triplicates [17,36,37].

Dye binding study

The microchannels formation by MN arrays in skin sample was evaluated using 1% w/v methylene blue dye. Before MN arrays application, the hairs on skin were carefully removed with disposable blade. The skin sample was pierced with MN arrays attached with TA-XT2 analyzer. Subsequently, the treated skin was applied with methylene blue staining for 5 min followed by removal of excessive stain using alcohol swabs and viewed again for pores formation using Leica EZ4D microscope (Wetzlar, Germany) [36]. Intact skin samples were used as control.

Histology studies

The histology of MNs untreated and microporated skin samples were observed using. VivoSight® high-resolution OCT Scanner. The skin layers were scanned at 8B-scans per second [17,35].

Skin integrity assessment

The dermatomed porcine skin samples (3 × 3 cm) were incubated in PBS for 30 min. Skin samples were placed on vertical Franz's cells in which the receptor compartment containing 5 mL, PBS 7.4 was stirred at 600 rpm. The skin barrier integrity was evaluated rapidly before and after MNs treatment via transepidermal water loss (TEWL) evaluation. Prior to TEWL measurement, the samples were allowed to hydrate in Franz cells for 1 h. TEWL values were calculated using a VapoMeter (Kuopio, Finland). After recording the basal values, skin samples were removed from cells and treated with MN arrays (600 μm, 361 MN/array) [13].

Water contents estimation

The water contents of MN arrays were calculated by Q500 Thermo gravimetric analyzer. MN array samples (5.0–10 mg) were run in the heating range of 20–300 °C at 10 °C/min under constant nitrogen flow. The obtained data were evaluated with Universal Analysis 2000 software [13].

In vitro *permeation study*

In vitro permeation study was conducted via Franz's diffusion setup for curcumin loaded 20% w/w PF127® gel samples across 400 μm skin samples. The drug permeation study was done across MNs untreated (non-porated) and MNs treated (microporated) skin samples.

Permeation across MNs untreated (non-porated) samples

The Franz diffusion setup comprised of a receptor compartment containing 5 mL, PBS (pH 7.4) at 37 ± 2 °C. Initially, the skin samples were placed on Franz cells and kept moistened for 1 h. The samples were then applied with PF127® based solution (20% w/w, 1000 μL) loaded with curcumin concentrations (0.1% and 0.3%). Each time, 500 μL sample was withdrawn and replaced with the same volume of PBS. The collected samples were used for drug quantification using Varian Cary 50 Bio UV-Visible spectrophotometer at 421 nm [13,17,35].

Permeation across MNs treated (microporated) skin samples

Similar procedure and apparatus setup were used for assessment of drug flux from gels across MN applied skin with slight amendments. Briefly, MNs were applied via the applicator (11 N). Then, 5 g stainless steel weight was again employed on embedded MN array and held for 1 min. The MNs were detached and porated samples were placed on the receptor compartment (5 mL, PBS, pH 7.4) at 600 rpm and keep thermostated at 37 ± 2 °C by water jacket. PF127® based solution (20% w/w, 1000 μL) loaded with curcumin concentrations (0.1% and 0.3%) was then applied on microporated skin samples, which get deposited in the micro conduits. At each time point, the samples (500 μL) were taken out from the Franz cells and refreshed with the equal volume of PBS. The collected samples were used for drug quantification using Varian Cary 50 Bio UV-Visible Spectrophotometer at 421 nm [17].

FTIR analysis

FTIR-4100 Series equipped with MIRacle™ software was utilized to study the network investigation of pure constituents and cross-linked MNs under 4000–600 cm^{-1} at 8.0 cm^{-1} resolution [17,38,39].

Scanning electron microscopic analysis

The morphology of MN arrays was evaluated using SEM analysis (Hitachi TM 3030 digital SEM, Chiyoda City, Japan). For SEM imaging, the MN arrays were placed on aluminum stubs and coated with gold/palladium [17,39,40]. The MN samples were scanned at various resolutions.

Statistical analysis

Data are presented as percentage or mean ± standard deviation (SD). The difference of parameters is statistically tested for significance by one-way analysis of variance (ANOVA) using GraphPad InStat or Origin programs. Statistically significant values were defined as $p < 0.05$.

Results and discussion

Phase transition of poloxamers

Phase transition of poloxamer solutions at body temperature is a key factor to be considered in order to ensure the *in situ* formation of MNs. AR2000 rheometer was used for phase conversion determination of poloxamer solutions (PF127 and P87) from sol–-gel state in flow and oscillatory modes, respectively. In flow mode, change in viscosity was evaluated over 25–40 °C at 0.1–10 s^{-1} shear rate via temperature and continuous ramp tests, respectively. In oscillatory mode, G' and G'' values with temperature change were investigated, which refers to phase transition temperature. These drug loaded poloxamer solutions located in pores will undergo from sol–gel state *in situ* and act as drug delivery depot by attaining MN shape.

Flow rheology

Temperature test. Change in viscosity over extended temperature range (25–40 °C) was measured to assess and confirm their phase change by conducting temperature ramp test. Poloxamer samples (PF127 and P87) in different ratios were formulated in cold distilled water and then tested for thermal gelation using AR-2000 rheometer. Table S1 refers to the composition of samples, gelation temperatures and viscosity at room and body temperature (37 °C).

In this study, poloxamers (PF127 and P87) were investigated at different compositions (15%, 20%, 25%, and 30% w/w) composed of diverse PEO/PPO molar ratios. Poloxamers are macromolecules with hydrophilic PEO ratios and central PPO hydrophobic component. Below LCGT, poloxamers aqueous solutions exist in low viscosity liquid form due to hydrophilic interaction of PEO components. However, at a certain concentrations above their LCGT, their viscosity increases sharply with small change in temperature. With increasing poloxamer contents, the PEO/PPO ratios in feed composition increased which in turn leads to faster micelles formation and gelation. Similar observations with Pluronics effect in response to temperature change were observed by Khan et al. [17]. Figure 2(A,B) shows the changes in viscosity profile of the poloxamers over temperature change (25–40 °C).

Continuous ramp test. The viscosity change under 0–10 1/s shear rate was evaluated at 30 °C. All the samples showed a progressive decrease in viscosity with increasing shear force. This decrease

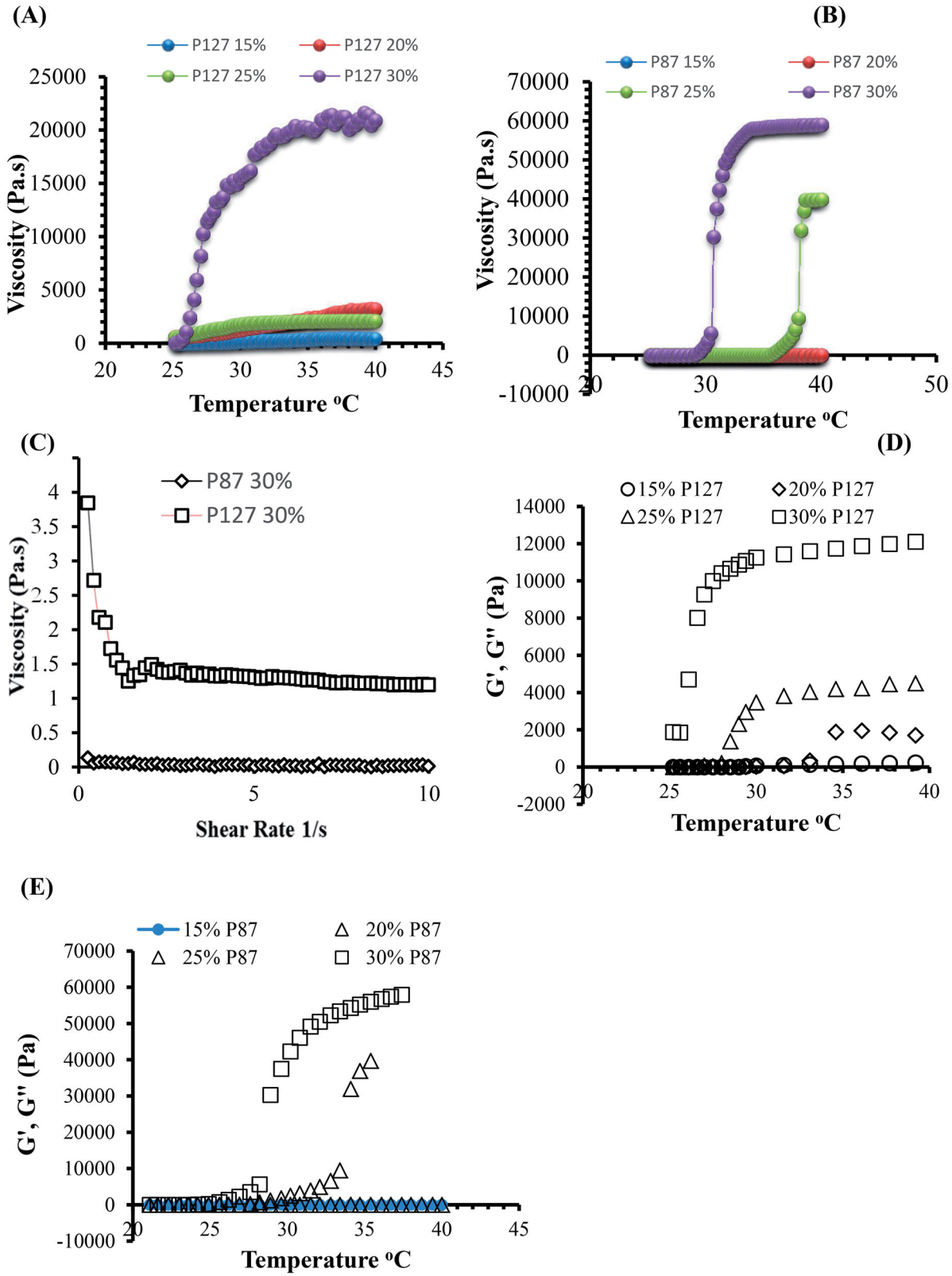

Figure 2. Changes in poloxamers viscosity profile over extended temperature range (25–40 °C) at diverse concentration: (A) PF®127, (B) P87, and (C) changes in poloxamers viscosity under shear rate (0.1–10 s^{-1}) at 25 °C. (D, E) Evaluation of G' and G'' of different poloxamers at different concentrations over 20–40 °C by oscillatory temperature ramp test. Data represent the mean ± standard deviation of three experiments.

occurred owing to breakage of physical cross links between the PPO groups [17]. Figure 2(C) shows the viscosity profile of samples with increasing shear rate.

Oscillatory temperature sweep test

Figure 2(D,E) indicates the change in G' and G'' values of poloxamer (PF127 and P87) with temperature variation. It was noted that at start G'' values were higher. However along temperature increase, sol–gel transition was seen with increased G' values that indicates the gel state of the samples. This thermal gelation is supposed owing to dehydration of PPO groups of poloxamers. Moreover, sol–gel conversion also depends on concentration of poloxamer used. As shown in Figure 2(D,E) at 15% w/w, no substantial change in G' was noted for both types of the poloxamer under 25–37 °C. Poloxamer 87 did not show any change in G' at 20% w/w concentration in the required temperature range (25–37 °C) as shown in Figure 2(E). However, PF127 exhibited an increase in G' values at 20% w/w concentration in the required temperature range (25–37 °C) as per results displayed in Figure 2(D). This is considered because of the higher hydrophobic PPO ratios in PF127 which quickly form micellization in response to temperature change and gel formation [17].

Effect of curcumin loading on LCGT of samples

In order to study the effect of curcumin on gelation temperatures of poloxamer formulations, the optimized poloxamer formulations were loaded with variable curcumin concentrations and subjected to rheological analysis. The effect of different curcumin contents on critical gelation temperature (CGT) of the poloxamer samples are listed in Table 1. It was noticed that with curcumin loading, the CGT of samples decreased correspondingly. This is because curcumin is hydrophobic in nature and with its loading, the hydrophobic interactions dominated over surrounding water molecules leading to thermal gelation at lower temperature.

Formulations of microneedle arrays

Several types of polymers were screened for the preparation of dissolving MN arrays with enhanced mechanical strength to determine their potential as source of microchannels formation in skin upon insertion. Table 2 enlisted the composition ratio of MN arrays. For MN arrays fabrication, laser-engineered silicone micromould templates as mentioned in Table 2 were used. The MN arrays were prepared from Gantrez® S-97, PEG10000, and gelatin B (Mw∼402.47 $gmol^{-1}$) in different weight ratio composition. However, MN arrays with high mechanical strength were selected [13,17]. Figure 3 indicates the digital microscopic images of MNs mentioned in Table 2.

Table 1. Effect of different curcumin (Cur) contents on gelation temperature of samples ($n = 3$, mean ± standard deviation).

		Concentration of curcumin (% w/w)		
Poloxamers (% w/w)		0	0.1	0.3
		Gelation temperature (°C)		
PF127	20	31.90	30.45 ± 0.09	28 ± 0.11
F 87	25	33.87	32 ± 0.7	30 ± 0.13

Mechanical strength determination

The TA Texture analyzer was used for the mechanical strength determination of MNs samples fabricated from various polymers (Gantrez® S-97, PEG10000, and gelatin B). The MN arrays were tested for 30 s against two predetermined compression forces (10 N and 20 N). The images of MN samples before and after mechanical testing are shown in Figure 3. From mechanical testing experiments, it was noticed that gelatin-based MNs displayed more brittle and fragile nature as a result of compression forces applications. Moreover, PG10000 MNs showed the highest strength against forces applied. Hence, it was concluded that PG10000 arrays provide the best MNs sample in lieu of their mechanical strength and can be used to create pores in skin. Notably during mechanical testing experiment, none of MN array was fractured or broken rather than compression of needles tips was detected [1,17]. Reduction in tips heights was considered and the data were presented as % loss vs. compression forces as displayed in Figure 4(A).

Insertion force determination

For formulations of *in situ* depot at skin temperature from poloxamers after MNs applications, it is necessary that the prepared dissolving MNs must have adequate mechanical stability to create pores upon application on skin. Texture analyzer was used for evaluating the insertion forces required for MN arrays. In this study, PG10000 MNs samples were selected owing to their highest mechanical strength. Figure 4(B) shows the insertion force/MN array vs. insertion depth. It was noticed that regardless of the applied force, >90% of each MN arrays successfully penetrated the neonatal porcine skin. However, the maximum penetration depth was observed for 361 needles in an array at higher forces. The pores creation in skin tissues were confirmed by methylene blue staining experiment.

Skin integrity assessment

The change in TEWL was evaluated for the barrier integrity assessment of skin after application of MN arrays. The VapoMeter was used which measures the rise in TEWL values after application. TEWL values indicate the skin rupturing grade and the base intact skin TEWL values were used as control values. The skin continuously loss minimal water from its surface. After SC barrier disruption, water loss increases owing to pores formation in skin. This difference in values indicates rupturing of the SC. As per results in Figure 4(C), it indicates that TEWL values improved significantly after MN arrays application which shows the evidence of interruption [1,17].

In situ *dissolution kinetics of MN arrays*

Since this study was aimed to produce micropores in skin using dissolving MN arrays as source of pores creation followed by drug

Table 2. Fabricated MN arrays feed composition and physical evaluation.

Sample codes	Samples composition	Weight ratio (% w/w)	Array	Total needles	Heights	Base widths
PG10000	Gantrez® S-97/PEG10000	10:7.5%	19 × 19	361	600 μm	300 μm
Gelatin	Gelatin B	15%	19 × 19	361	600 μm	300 μm

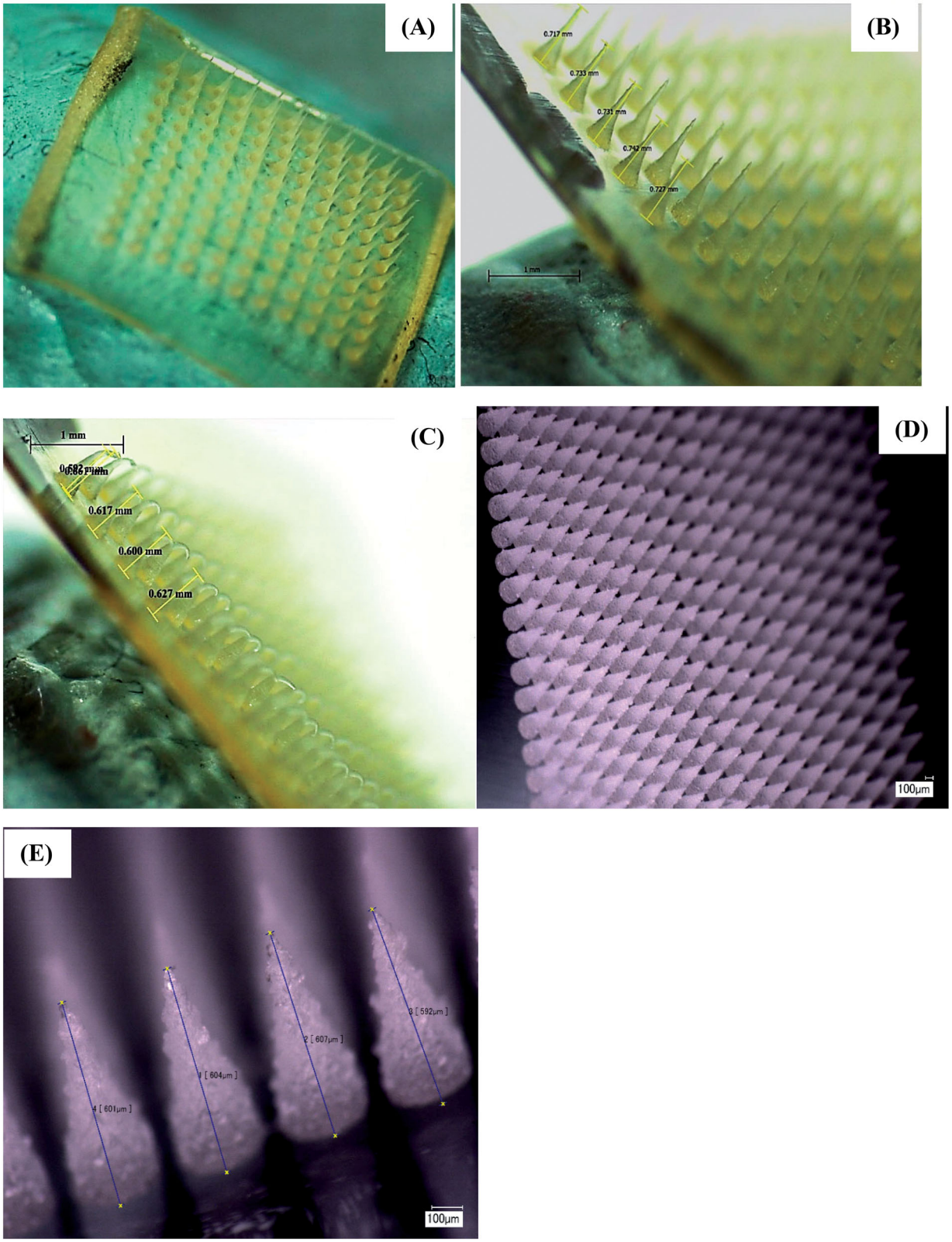

Figure 3. Fabricated MNs microscopic images of (A, B) gelatin (15%) at low and high resolutions. (C) Gelatin based MNs after applying predefined compression forces. (D, E) Gantrez® S-97 and PEG10000 (PG10000 MN arrays) at low and high resolutions.

loaded poloxamer solution application, the *in situ* dissolution fate of MN arrays is critical to be considered. *In situ* dissolution study of MN arrays was conducted to observe the fate or *in situ* dissolution and select the best MN array formulation reported in Table 2. Several factors governed over the mechanical strength of MN arrays including polymers molecular weight, concentration, polymer type, and moisture contents [1,17]. The *in situ* dissolution kinetics of fabricated MN arrays is shown in Figure 4(D). It was observed from the results that gelatin 15% w/w based MN arrays displayed quicker dissolution in skin fluids. The results displayed

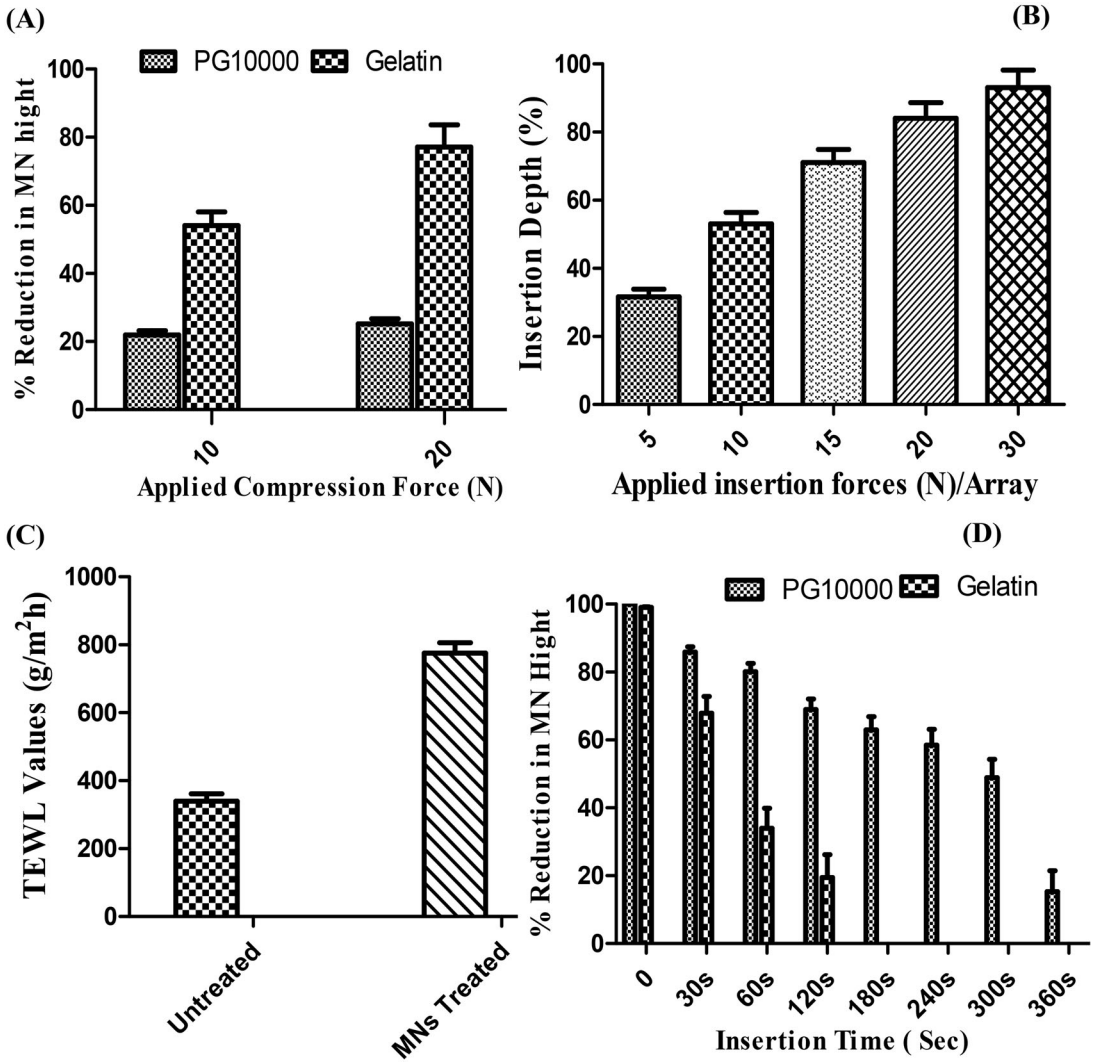

Figure 4. Mechanical strength evaluation of fabricated MNs representing the percent reduction in MNs heights (mean ± SD of $n = 3$) (A), effect of insertion forces on penetration of MNs into skin, (B) skin integrity assessment of untreated and MNs treated by calculating TEWL values (C), and *in situ* dissolution profile of MN arrays in skin (mean ± SD of $n = 3$) (D).

that gelatin based MNs start dissolution in 30 s and dissolved completely in 120 s. These results of gelatin MN arrays are in good agreement with mechanical stability which indicates the brittle solid nature with less mechanical strength. On the other hand, it was observed that PG10000 MNs showed similar dissolution pattern in the interstitial fluid but displayed slower rate of dissolution in comparison to gelatin MN arrays. From the results, it was concluded that PG10000 MNs showed complete dissolution in 360 s which designate their higher mechanical stability owing to cross-linked nature.

Histology study

VivoSight® high-resolution OCT scanner was used for the histological study of the neonatal porcine skin sections which provided evidence of perforations with PG10000 MN arrays. First, intact skin layers were observed with VivoSight® scanner in untreated skin sample as shown in Figure 5(A,B). The OCT pictures of the skin treated with PG10000 MNs indicated that MN arrays pierce SC layer shown in Figure 5(C), infiltrate the epidermis and goes to dermis layer as indicated in Figure 5(D,E). It is shown that curcumin-loaded poloxamers solution will pass on to pores after application on skin, convert into gel *in situ* at body temperature and form curcumin delivery depot [17].

OCT imaging for penetration depth determination

MN arrays penetration (PG10000 and gelatin B 15% w/w) into the skin was assessed using VivoSight® Scanner. Figure 5(D,E) shows the OCT images of *in vitro* insertion and depth of penetration of PG10000 and gelatin B MN arrays formulations. The PG10000 formulation presented good insertion ability in full thickness skin tissue owing to their mechanical stability. Table S2 indicates the MNs heights (μm) and average depth of penetration (μm) into the skin tissues.

Dye binding study

Methylene blue dye (1%) due to its hydrophilic nature was used as basis of pores visualization in skin. The pores created were stained with 1% methylene blue dye. Owing to its hydrophilic nature, it was absorbed by the interstitial fluid in pores. Figure 6(A,B) refers to the untreated and porous skin samples. Staining

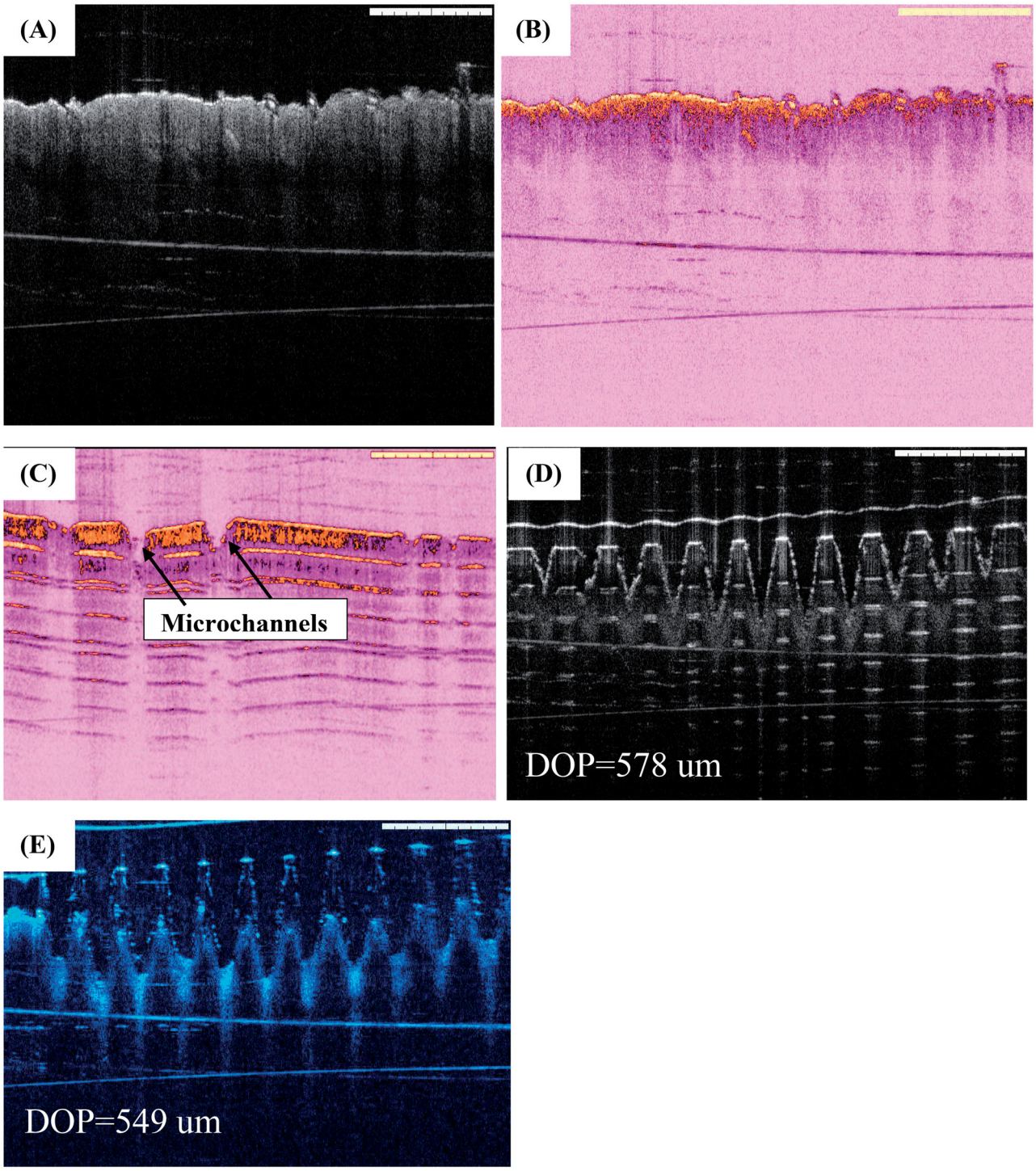

Figure 5. Histological images of untreated skin (A, B), MNs treated skin piercing SC layer (C), pores and micro channels formation of PG10000 MNs in underlying layers of skin (D), and pores and micro channels formation of gelatin B MNs in underlying layers of skin (E).

affirmed the piercing of SC layer and consistency which indicate the sharpness of the MN arrays [1,17].

Ex vivo *permeation study*

The *ex vivo* permeation of drug was tested from optimized poloxamer solution loaded with variable drug contents across MNs untreated and treated skin samples. The *in vitro* drug permeation was carried out using vertical Franz's diffusion cell across skin at 37 ± 1 °C. The permeation was investigated for optimized poloxamer formulations (20% w/w PF127® sample, 1000 µL) loaded with variable drug concentrations (0.1% and 0.3%). The drug permeation was first investigated through intact skin. Then skin samples were punctured with PG10000 (600 µm) because of their good mechanical strength, and then applied curcumin loaded PF127® poloxamer solution. The accumulation of permeated drug in receptor compartment was noticed with time [41,42].

It was observed that MNs treated skin samples showed a high permeation of curcumin and in more sustained fashion for both concentrations used. It was found from the delivery profile that 20% w/w PF127® gel formulation containing 0.1% curcumin

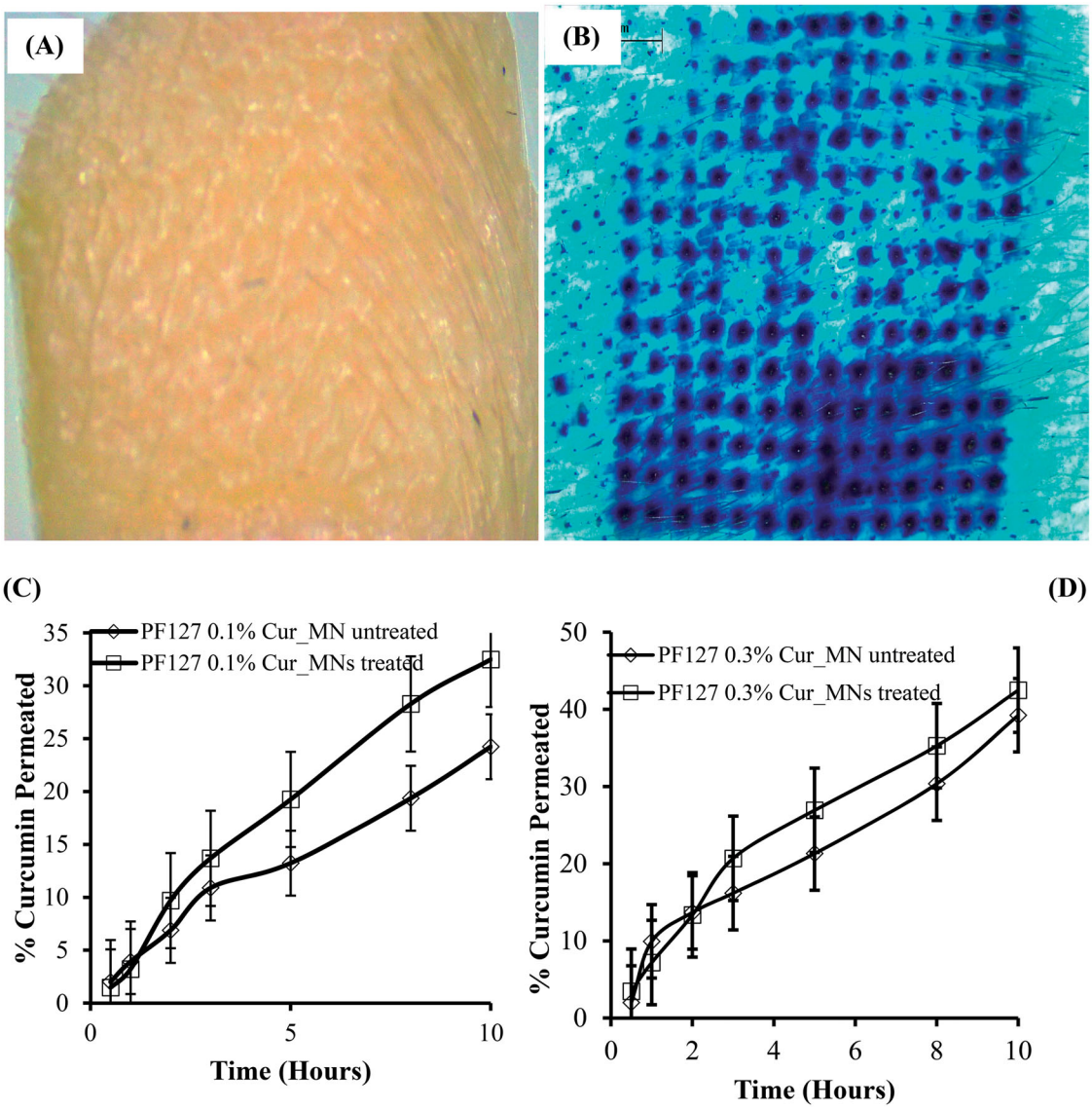

Figure 6. Microchannels visualization via staining with methylene blue dye. (A) Untreated neonatal porcine skin sample. (B) Stained skin after treatment with PG10000 MN arrays. (C) *In vitro* cumulative permeation profile of 0.1% curcumin loaded gels across intact (350 μm) and microporated skin samples at same concentration. (D) Curcumin permeation profile of 0.3% gels across intact and porated samples at same concentration. Results are the mean ± SD ($n = 3$).

provided 49 ± 0.87% across MNs untreated samples and release was saturated at 36 h. On the other hand across microporated samples, 72 ± 0.60% permeation of drug was observed for 60 h at similar concentration. Similarly for 0.3% curcumin loaded gel formulation, 71 ± 0.93% drug permeation was observed across MNs untreated and the release occurred till 60 h, while in case of MNs treated samples, 91 ± 0.98% drug permeation was found for longer duration, i.e. 98 h. It was concluded from permeation experiment that drug loaded 20% w/w PF127® gel formulation showed a high release and permeation across MNs treated skin samples at both concentrations. This is because after MNs treatment the poloxamers solution loaded with therapeutic agent flow inside the microconduits produced and diffuse deeper to the subcutaneous skin layer. The poloxamers solution due to their thermogelling property at skin temperature form depot for curcumin in the microchannels produced. These *in situ* forming depot loaded with drug diffuse deeper in skin layers and released the drug in more constant fashion. On the other hand, drug delivery across MNs untreated skin samples was also observed in controlled fashion; however, the delivery was saturated at comparatively earlier time. This is probably suggested because of the difficulty in diffusion of hydrophobic drug molecules through hydrophilic dermis layer, which hinders the permeation of drug molecules. Figure 6(C,D) refers to the cumulative permeation of curcumin from 20% w/w PF127® based formulations across intact and porated skin samples at both concentrations.

In this current study, for the first time, the *in situ* formation of depot MNs using different poloxamers was investigated at skin or body temperature owing to their good thermogelling property. Moreover, it was concluded from the permeation study that the permeation of hydrophobic drug (curcumin) across MNs treated skin from *in situ* forming MNs that occur for longer duration in comparison to untreated skin samples.

Confocal microscopic study

In order to track the distribution of curcumin in MNs treated skin samples after the termination of permeation study, confocal laser microscopic analysis was carried out. The skin samples were stained with CellMask Deep Red on porated site and were

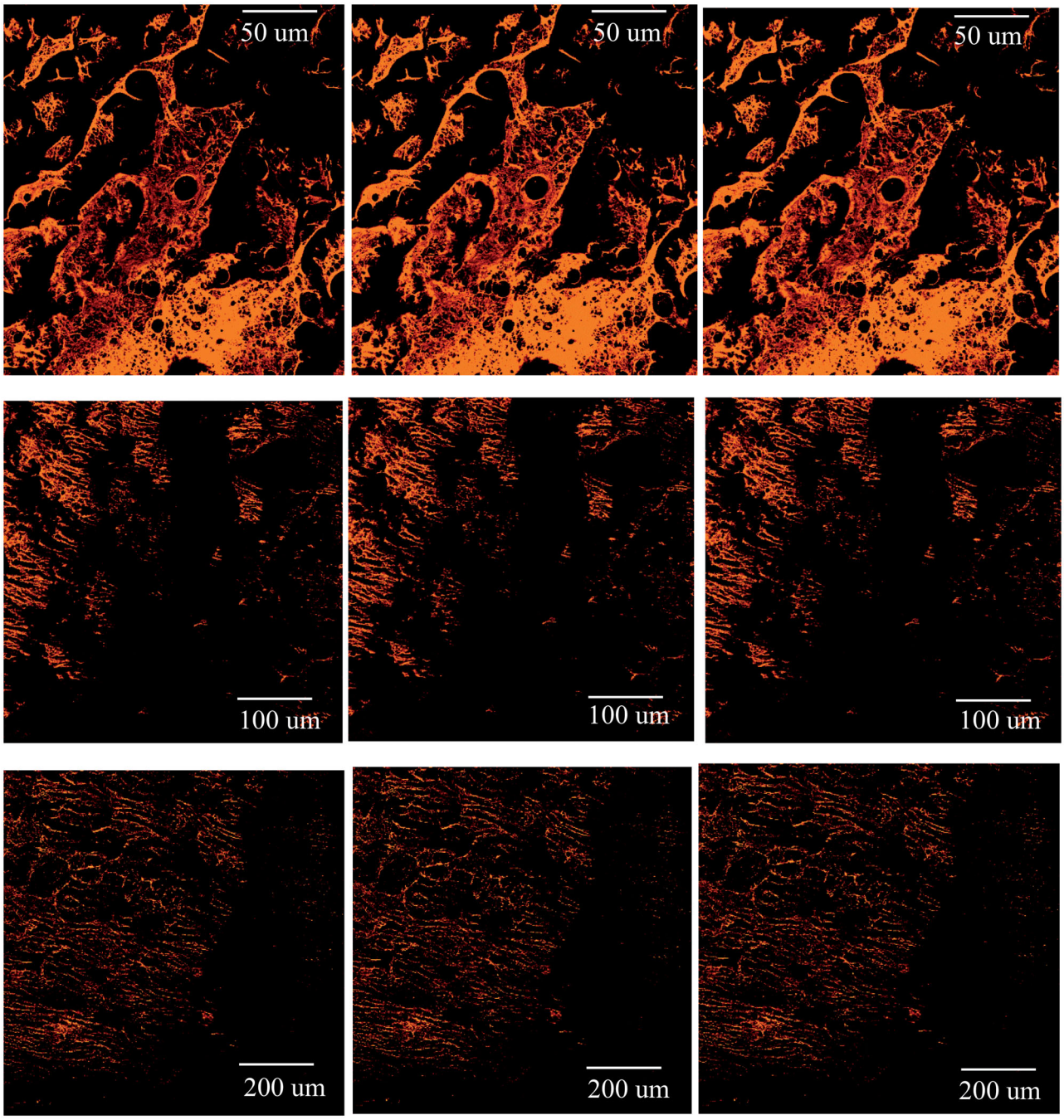

Figure 7. Confocal microscopic images (z-track series) of curcumin distribution in microporated skin tissues.

subjected to confocal scanning. We used Z stack series that captures skin images in horizontal sequence at variable depth (*z*). From florescence signals, it was observed that 0.3% curcumin loaded in 20% w/w PF127® gel formulation applied on microporated skin samples diffuse deeper in skin layers as shown in Figure 7. This is owing to piercing the SC layer (10–15-μm thick) by PG10000 MNs treatment followed by diffusion to underlying epidermis and dermis layers (50–100-μm thick). Moreover, decrease in florescence intensity was observed with increasing channels depth. Altogether from confocal scanning, it was concluded that poloxamer solution loaded with curcumin infiltered deeper into the skin tissues after treatment with PG10000 MNs due to creation of microchannels in skin [1,17].

FT-IR spectroscopic analysis

The network structure formation and the physical crosslinking between the polymers was evaluated using infrared spectroscopy technique. Figure S1 illustrates the FTIR spectra of the pure ingredients and PG10000 MNs. In FTIR spectra of pure Gantrez® S-97 sample, single peak at ~1723 cm^{-1} attributed to acid carbonyl groups. PG10000 spectrum shows three altered carbonyl peaks. The first peak at ~1321 cm^{-1} is attributed to presence of anhydride groups. The second carbonyl peak (1732 cm^{-1}) refers to the ester carbonyl group. The third carbonyl peak detected at ~1478 cm^{-1} shows acid carbonyl group. In the FTIR spectra of pure gelatin, band of N–H stretching appeared at 2416 cm^{-1}.

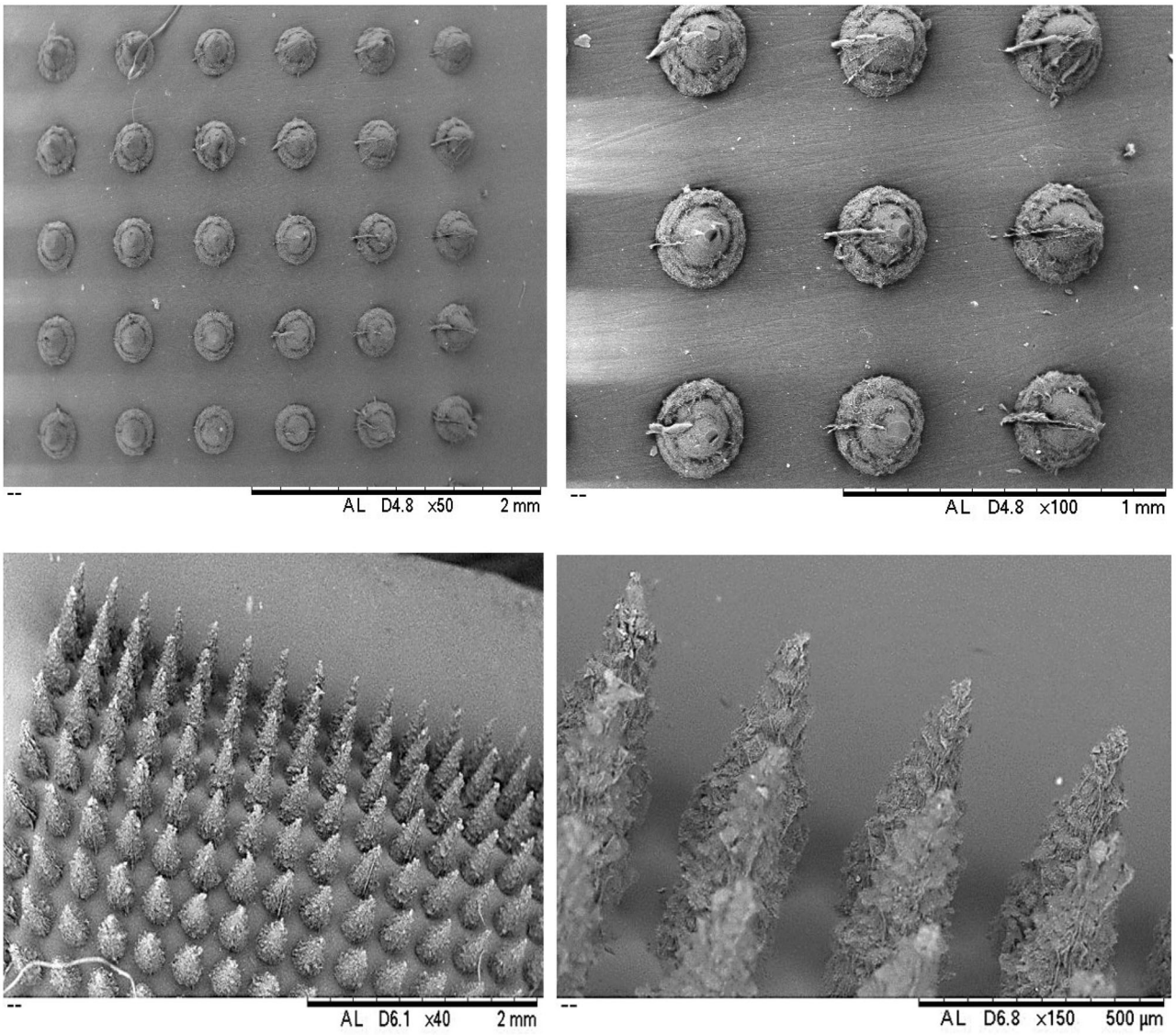

Figure 8. Scanning electron microscopy of gelatin MNs arrays: (A) ×50 magnification, (B) ×100 magnification, (C) PG10000 MN arrays at ×40 magnification, and (D) ×150 magnification.

The N–H bending was observed at 1429 cm^{-1}. Aliphatic C–H stretching is detected at 3126 cm^{-1}, while aliphatic C–H bending is detected at 1335 and 1387 cm^{-1}, respectively. In the FTIR spectra of gelatin MNs, N–H stretching vibration consumed during the crosslinking reaction and assumed to create a new structure.

Moisture contents determination

The mechanical properties of MN arrays are highly affected by the presence of moisture or water contents in formulations. The moisture contents greatly affect the brittleness, flexibility, and hardness of MNs. Thermogravimetric analysis (TGA) was used for moistures determinations of MNs and the results are displayed in Table S2. It was concluded from the results that gelatin-based MN arrays showed lower moisture contents which in turn indicate their dry, brittle, and rigid nature. In contrast, PG10000 MN arrays displayed higher moisture contents as shown in Table S2. Some other factors such as polymer type, concentration, molecular weights, and overall lab conditions also facilitate the presence of moisture contents.

SEM analysis

The MNs morphology was analyzed by SEM at various resolutions. SEM analysis showed that the needles were sharp, intact, and hard to cause pores. Based on their sharp morphology, it is suggested that these MNs can easily pierce the SC layer of skin. Figure 8 refers to the SEM images of the fabricated MNs.

Conclusion

Taking the advantage of phase transition temperature of poloxamers and their *in situ* gelation at body temperature, a novel approach was adopted for the controlled delivery of pharmaceuticals via microporated skin after treatment of non-soluble crosslinked MN arrays. In the current study, different poloxamer grades (PF127 and P87) were used to design novel *in situ* forming depots in micropores of skin created by MNs treatment. Rheological tests on poloxamers were performed to confirm the phase conversion property at skin temperature (32 °C). Microneedle arrays were fabricated from Gantrez® S-97, PEG10000, and gelatin B using

laser-engineered silicone micromoulds and were further used as source of microporation in skin. The MNs were characterized for stability, insertion forces, *in situ* dissolution study and moisture contents. The optimized MNs were selected on the basis of their non-soluble cross-linked nature evaluated via dissolution kinetics. The pores formation and porcine skin penetration of MNs arrays were confirmed via OCT and dye binding study. It was concluded from *in vitro* permeation study that curcumin permeation occurred in sustained fashion and for prolonged time across MNs treated skin samples in comparison to MNs untreated skin. Confocal laser microscopic analysis confirmed the distribution of curcumin with greater concentration in microporated skin tissues. Structural characterization of fabricated MNs confirmed their crosslinked nature. While the morphology of MNs was assessed using SEM. Altogether it was concluded that phase conversion property of Pluronics can be used to form *in situ* MNs assisted depots in the porated site at skin and will provide the controlled delivery for prolonged time of curcumin loaded in poloxamers formulation.

Acknowledgements

S. Khan and M. U. Minhas highly acknowledge Higher Education Commission of Pakistan for providing financial support for conducting this study through IRSIP at the School of Pharmacy, Queens University Belfast UK.

Disclosure statement

No potential conflict of interest was reported by the author(s).

Funding

The author(s) reported there is no funding associated with the work featured in this article.

ORCID

Samiullah Khan http://orcid.org/0000-0001-7004-9393
Raghu Raj Singh Thakur http://orcid.org/0000-0001-7582-2082

References

[1] Thakur RRS, Fallows SJ, McMillan HL, et al. Microneedle-mediated intrascleral delivery of *in situ* forming thermoresponsive implants for sustained ocular drug delivery. J Pharm Pharmacol. 2014;66(4):584–595.
[2] Nguyen KT, Ita KB, Parikh SJ, et al. Transdermal delivery of captopril and metoprolol tartrate with microneedles; [cited 2017 Nov 10]. Available from: http://www.ingentaconnect.com/content/ben/ddl/2014/00000004/00000003/art00006
[3] Nguyen J, Ita K, Morra M, et al. The influence of solid microneedles on the transdermal delivery of selected antiepileptic drugs. Pharmaceutics. 2016;8(4):33.
[4] Sullivan SP, Koutsonanos DG, del Pilar Martin M, et al. Dissolving polymer microneedle patches for influenza vaccination. Nat Med. 2010;16(8):915–920.
[5] Scott JA, Banga AK. Cosmetic devices based on active transdermal technologies. Ther Deliv. 2015;6(9):1089–1099.
[6] Matsuo K, Yokota Y, Zhai Y, et al. A low-invasive and effective transcutaneous immunization system using a novel dissolving microneedle array for soluble and particulate antigens. J Control Release. 2012;161(1):10–17.
[7] Naito S, Ito Y, Kiyohara T, et al. Antigen-loaded dissolving microneedle array as a novel tool for percutaneous vaccination. Vaccine. 2012;30(6):1191–1197.
[8] Gomaa YA, Garland MJ, McInnes F, et al. Laser-engineered dissolving microneedles for active transdermal delivery of nadroparin calcium. Eur J Pharm Biopharm. 2012;82(2):299–307.
[9] Carey JB, Vrdoljak A, O'Mahony C, et al. Microneedle-mediated immunization of an adenovirus-based malaria vaccine enhances antigen-specific antibody immunity and reduces anti-vector responses compared to the intradermal route. Sci Rep. 2014;4:1–13.
[10] Fourtanier A, Berrebi C. Miniature pig as an animal model to study photoaging. Photochem Photobiol. 1989;50(6):771–784.
[11] Sivaraman A, Banga AK. Novel in situ forming hydrogel microneedles for transdermal drug delivery. Drug Deliv Transl Res. 2017;7(1):16–26.
[12] Nguyen HX, Banga AK. Fabrication, characterization and application of sugar microneedles for transdermal drug delivery. Ther Deliv. 2017;8:249–264.
[13] Raj R, Thakur S, Tekko IA, et al. Rapidly dissolving polymeric microneedles for minimally invasive intraocular drug delivery. Drug Deliv Transl Res. 2016;6(6):800–815.
[14] Tuan-Mahmood TM, McCrudden MTC, Torrisi BM, et al. Microneedles for intradermal and transdermal drug delivery. Eur J Pharm Sci. 2013;50:623–637.
[15] Park JH, Allen MG, Prausnitz MR. Biodegradable polymer microneedles: fabrication, mechanics and transdermal drug delivery. J Control Release. 2005;104(1):51–66.
[16] Aoyagi S, Izumi H, Fukuda M. Biodegradable polymer needle with various tip angles and consideration on insertion mechanism of mosquito's proboscis. Sens Actuators A Phys. 2008;143:20–28.
[17] Khan S, Minhas MU, Tekko IA, et al. Evaluation of microneedles-assisted in situ depot forming poloxamer gels for sustained transdermal drug delivery. Drug Deliv Transl Res. 2019;9:764–782.
[18] Tobin KV, Fiegel J, Brogden NK. Thermosensitive gels used to improve microneedle-assisted transdermal delivery of naltrexone. Polymers. 2021;13:933.
[19] Bhattaccharjee S, Beck-Broichsitter M, Banga AK. In situ gel formation in microporated skin for enhanced topical delivery of niacinamide. Pharmaceutics. 2020;12:472.
[20] Khan S, Akhtar N, Minhas MU, et al. pH/thermo-dual responsive tunable in situ cross-linkable depot injectable hydrogels based on poly(N-isopropylacrylamide)/carboxymethyl chitosan with potential of controlled localized and systemic drug delivery. AAPS PharmSciTech. 2019;20:119.
[21] Khan S, Minhas MU, Ahmad M, et al. Self-assembled supramolecular thermoreversible β-cyclodextrin/ethylene glycol injectable hydrogels with difunctional pluronic 127 as controlled delivery depot of curcumin. Development, characterization and in vitro evaluation. J Biomater Sci Polym Ed. 2018;29(1):1–34.
[22] Chung HJ, Lee Y, Park TG. Thermo-sensitive and biodegradable hydrogels based on stereocomplexed pluronic multiblock copolymers for controlled protein delivery. J Control Release. 2008;127(1):22–30.
[23] Nasir F, Iqbal Z, Khan JA, et al. Development and evaluation of diclofenac sodium thermoreversible subcutaneous drug delivery system. Int J Pharm. 2012;439(1–2):120–126.

[24] Khan S, Anwar N. Gelatin/carboxymethyl cellulose based stimuli-responsive hydrogels for controlled delivery of 5-fluorouracil, development, in vitro characterization, in vivo safety and bioavailability evaluation. Carbohydr Polym. 2021;257:117617.
[25] Mad-Ali S, Benjakul S, Prodpran T, et al. Characteristics and gelling properties of gelatin from goat skin as affected by drying methods. J Food Sci Technol. 2017;54(6):1646–1654.
[26] Chen JP, Leu YL, Fang CL, et al. Thermosensitive hydrogels composed of hyaluronic acid and gelatin as carriers for the intravesical administration of cisplatin. J Pharm Sci. 2011; 100(2):655–666.
[27] Alaikov T, Konstantinov SM, Tzanova T, et al. Antineoplastic and anticlastogenic properties of curcumin. Ann N Y Acad Sci. 2007;1095(1):355–370.
[28] O'Connell MA, Rushworth SA. Curcumin: potential for hepatic fibrosis therapy? Br J Pharmacol. 2008;153(3):403–405.
[29] Bruck R, Ashkenazi M, Weiss S, et al. Prevention of liver cirrhosis in rats by curcumin. Liver Int. 2007;27(3):373–383.
[30] Sowasod N, Nakagawa K, Tanthapanichakoon W, et al. Development of encapsulation technique for curcumin loaded O/W emulsion using chitosan based cryotropic gelation. Mater Sci Eng C. 2012;32(4):790–798.
[31] Khan S, Akhtar N, Minhas MU, et al. A difunctional Pluronic®127-based in situ formed injectable thermogels as prolonged and controlled curcumin depot, fabrication, in vitro characterization and in vivo safety evaluation. J Biomater Sci Polym Ed. 2021;32(3):281–319.
[32] Derakhshandeh K, Fashi M, Seifoleslami S. Thermosensitive Pluronic® hydrogel: prolonged injectable formulation for drug abuse. Drug Des Devel Ther. 2010;4:255–262.
[33] Baskan T, Tuncaboylu DC, Okay O. Tough interpenetrating pluronic F127/polyacrylic acid hydrogels. Polymer. 2013; 54(12):2979–2987.
[34] Moreira HR, Munarin F, Gentilini R, et al. Injectable pectin hydrogels produced by internal gelation: pH dependence of gelling and rheological properties. Carbohydr Polym. 2014;103:339–347.
[35] Modepalli N, Shivakumar HN, McCrudden MTC, et al. Transdermal delivery of iron using soluble microneedles: dermal kinetics and safety. J Pharm Sci. 2016;105(3): 1196–1200.
[36] Larrañeta E, Stewart S, Fallows SJ, et al. A facile system to evaluate in vitro drug release from dissolving microneedle arrays. Int J Pharm. 2016;497(1–2):62–69.
[37] Donnelly RF, Garland MJ, Morrow DIJ, et al. Optical coherence tomography is a valuable tool in the study of the effects of microneedle geometry on skin penetration characteristics and in-skin dissolution. J Control Release. 2010; 147:333–341.
[38] Mccrudden MTC, Zaid A, Mccrudden CM, et al. Design and physicochemical characterisation of novel dissolving polymeric microneedle arrays for transdermal delivery of high dose, low molecular weight drugs. J Control Release. 2014; 180:71–80.
[39] Ripolin A, Quinn J, Larrañeta E, et al. Successful application of large microneedle patches by human volunteers. Int J Pharm. 2017;521(1–2):92–101.
[40] Khan S, Akhtar N, Minhas MU. Fabrication, rheological analysis, and in vitro characterization of in situ chemically cross-linkable thermogels as controlled and prolonged drug depot for localized and systemic delivery. Polym Adv Technol. 2019;30:755–771.
[41] Hathout RM, Woodman TJ, Mansour S, et al. Microemulsion formulations for the transdermal delivery of testosterone. Eur J Pharm Sci. 2010;40(3):188–196.
[42] ElMasry SR, Hathout RM, Abdel-Halim M, et al. *In vitro* transdermal delivery of sesamol using oleic acid chemically-modified gelatin nanoparticles as a potential breast cancer medication. J Drug Deliv Sci Technol. 2018;48:30–39.